Diffusing Colloidal Probes of Protein and Synthetic Macromolecule Interactions

W. Neil Everett,* Hung-Jen Wu,[†] Samartha G. Anekal,[†] Hung-Jue Sue,* and Michael A. Bevan[†]

*Department of Mechanical Engineering, and [†]Department of Chemical Engineering, Texas A&M University, College Station, Texas 77843

ABSTRACT   A new approach is described for measuring kT and nanometer scale protein-protein and protein-synthetic macromolecule interactions. The utility of this method is demonstrated by measuring interactions of bovine serum albumin (BSA) and copolymers with exposed polyethyleneoxide (PEO) moieties adsorbed to hydrophobically modified colloids and surfaces. Total internal reflection and video microscopy are used to track three-dimensional trajectories of many single diffusing colloids that are analyzed to yield interaction potentials, mean-square displacements, and colloid-surface association lifetimes. A criterion is developed to identify colloids as being levitated, associated, or deposited based on energetic, spatial, statistical, and temporal information. Whereas levitation and deposition occur for strongly repulsive or attractive potentials, association is exponentially sensitive to weak interactions influenced by adsorbed layer architectures and surface heterogeneity. Systematic experiments reveal how BSA orientation and PEO molecular weight produce adsorbed layers that either conceal or expose substrate heterogeneities to generate a continuum of colloid-surface association lifetimes. These measurements provide simultaneous access to a broad range of information that consistently indicates purely repulsive BSA and PEO interactions and a role for surface heterogeneity in colloid-surface association. The demonstrated capability to measure nonspecific protein interactions provides a basis for future measurements of specific protein interactions.

INTRODUCTION

Understanding nonspecific interactions of synthetic and biological macromolecules is of great importance to traditional medicine and the interface of nanotechnology and biology (1,2). Although nearly all of medicine necessarily involves interactions of synthetic and biological systems, many emerging applications require robust integration of materials on molecular to micron scales such as novel therapeutics (e.g., nanoparticles, gene delivery), sensors (e.g., insulin), biomolecular chips (e.g., DNA, protein), cellular diagnostics (e.g., microfluidic, arrays), and tissue engineering. Very generally, a net repulsive intermolecular interaction is often required to prevent nonspecific binding, adsorption, or aggregation of proteins to other proteins and synthetic materials to allow retention of specific interactions that are the origin of unique biological function both in vitro and in vivo.

Techniques for interrogating adsorbed protein and synthetic macromolecular interactions in physiological media can generally be categorized as falling into several mutually exclusive categories based on fundamental approaches and accessible information (3). Scanning probe methods externally manipulate separation between adsorbed macromolecule coated substrates and gauge interactions via displacements of actual (e.g., AFM cantilevers) or effective (e.g.,optical traps) springs to yield direct, high resolution, high energy/force measurements (4–12). In contrast, spectroscopic methods quantify interactions between soluble and surface bound species via changes in interfacial spectroscopic signatures (e.g., fluorescence, refractive index) to produce nonintrusive, statistically significant measures of equilibrium binding with imaging capabilities (12–18). Another distinct measurement type, most closely related to the method in this article, involves passively monitoring Brownian colloids near surfaces bearing adsorbed/conjugated biomacromolecules typically to characterize nonspecific, long-range interactions or tethered chain mechanics (19–25). This is not an exhaustive review but highlights several complementary approaches to quantitatively measure protein and macromolecule interactions.

In this article, we report a novel method using micron sized colloids to directly and nonintrusively measure kT and nanometer scale interactions between adsorbed bovine serum albumin (BSA) and copolymers with polyethyleneoxide (PEO) moieties. By integrating total internal reflection (TIRM) and video (VM) microscopies (26–28), three-dimensional (3D) Brownian excursions of many single colloids bearing adsorbed BSA or copolymers with exposed PEO moieties are monitored near similarly coated wall surfaces (see Fig. 1). Statistical mechanical and dynamic analyses of colloid distributions (26–31) and trajectories (32–34) yield normal potential energy profiles (PEP), lateral mean-square displacements (MSD), and colloid-surface association (CSA) lifetimes. Simultaneous single and ensemble average analyses of many diffusing colloids allow for a consistent and unambiguous interpretation of spatial, statistical, temporal, and energetic aspects of BSA-PEO mediated colloid-surface interactions. By passively monitoring Brownian excursions of diffusing colloids on surfaces, this new technique exploits natural gauges for time (a^2/D), energy (kT), force (fN), and
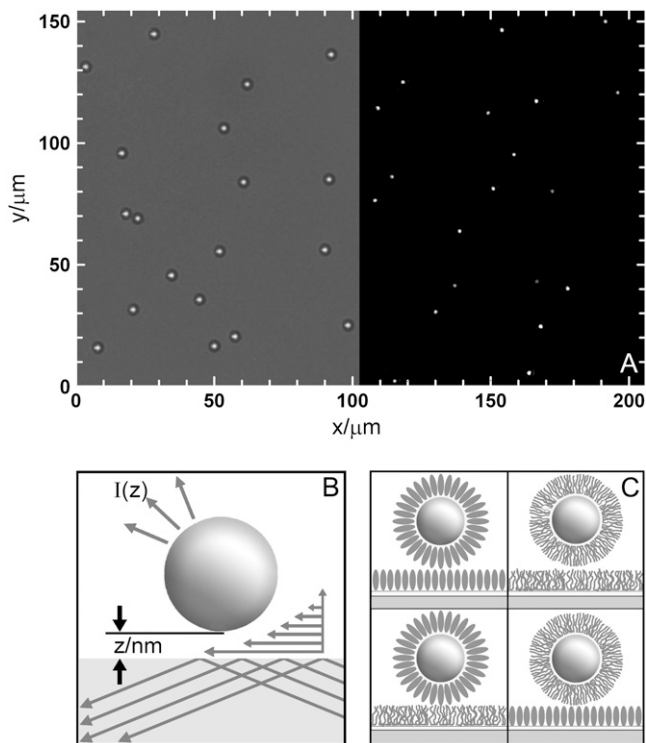
FIGURE 1 (A) Total internal reflection and video microscopy of 2.2 μm silica colloids levitated above a microscope slide with and without transmitted light. (B) Schematic of total internal reflection, evanescent wave, and colloid scattering. (C) Schematic of BSA (ellipsoids) and PEO (brush layer) configurations on chemically modified surfaces.

length (nm) when interrogating protein-synthetic macromolecule interactions. Successful measurement of nonspecific interactions using this technique provides a basis to measure specific interactions in integrated synthetic-biomolecular materials, devices, and systems.

MATERIALS AND METHODS

Colloid, macromolecule, and surface preparation

Glass microscope slides (Gold Seal, Corning, NY) were soaked in piranha solution (3:1 H_2SO_4:H_2O_2) for 1 h followed by rinsing with deionized water. Slide surfaces were modified with octadecyltrichlorosilane (OTS) and 3-aminopropyltriethoxysilane (APS) using standard protocols (35). Au films were prepared by evaporating 5 nm of chromium and 5 nm of Au onto slides at 0.1 nm/s using a metal evaporator chamber (Auto 306, BOC Edwards, Wilmington, MA). 2.2 μm silica colloids ($\rho = 1.96$ g/ml) were purchased from Bangs Laboratories (Fishers, IN) and washed with deionized water. Silica colloids were modified with 1-octadecanoic acid (ODA) using a literature method (36) and with APS by adding a 50 mM APS toluene solution to an equal volume of silica colloids suspended in toluene by periodic sonication. Modified silica colloids were transferred to aqueous media by repeated centrifugation and resuspension in deionized water.

Three polyethyleneoxide-polypropyleneoxide-polyethyleneoxide copolymers (Pluronic, BASF, Wyandotte, MI) were used with similar block ratios but different nominal molecular weights (F68-3400/1700/3400, F127-4400/3800/4400, F108-5400/3300/5400). To develop compact and meaningful notation for each copolymer, abbreviations are PEO3k (F68), PEO4k

(F127), and PEO5k (F108) based on PEO block molecular weights. BSA was γ-globulin-free (Sigma-Aldrich, St. Louis, MO). Aqueous phosphate buffer (Fisher Scientific, Pittsburgh, PA) solutions of PEO-PPO-PEO copolymers and BSA were prepared at 1 mg/ml. BSA and Pluronic were adsorbed to silica colloids for 12 h on a shaker and were adsorbed to slide surfaces for 6 h in a flow cell using a syringe pump (New Era Pumps, Wantagh, NY).

Colloid tracking and scattering

Colloidal evanescent wave scattering was monitored with a 12-bit CCD camera (ORCA-ER, Hamamatsu, Japan) on an optical microscope (Axioplan 2, Zeiss, Germany). The camera was operated in 8-binning mode in conjunction with a 40× objective (Achroplan, numerical aperture 0.60) to yield 43 frames/s with a spatial resolution of 168 × 128 pixels (1215 nm/pixel). A 15-mW, 632.8 nm Helium-Neon laser (Melles Griot, Carlsbad, CA) was used to generate an evanescent wave decay length of $\beta^{-1} = 113$ nm in a flow cell optically coupled to a 68° dovetail prism (Reynard Corp., San Clemente, CA) placed on a three-point leveling stage. Image analysis algorithms coded in Fortran were used to track and integrate evanescent wave scattering from each colloid (26–28).

Colloid-surface potentials

As levitated colloids diffuse over a surface, their instantaneous heights, h, can be directly measured from their scattering intensity, $I(h)$, in an evanescent wave using (37)

$$h - h_{\mathrm{ref}} = \beta^{-1} ln[I(h_{\mathrm{ref}})/I(h)], \qquad (1)$$

where $I(h_{\mathrm{ref}})$ is the scattering intensity at a reference height, and β^{-1} is determined by the laser's incident angle and the incident and transmitted media refractive indices. A time averaged single-colloid or ensemble-average height histogram, $p(h)$ (26,28), can be generated from many height observations and related to the PEP, $u(h)$, using Boltzmann's equation as (26–28)

$$u(h) - u(h_{\mathrm{ref}}) = kT \, ln[p(h_{\mathrm{ref}})/p(h)], \qquad (2)$$

where $p(h_{\mathrm{ref}})$ is a reference height probability determined by a reference height potential, $u(h_{\mathrm{ref}})$.

Colloid surface diffusion and migration

The lateral, $D_{\parallel}(h)$, and normal, $D_{\perp}(h)$, diffusivities of single colloids near planar surfaces with particle-surface separation, h, are given by (34)

$$D_{\parallel}(h) = D_0 f_{\parallel}(h), D_{\perp}(h) = D_0 f_{\perp}(h), \qquad (3)$$

where D_0 is the bulk single colloid diffusivity, $D_0 = (kT)/(6\pi\mu a)$, μ is the medium viscosity, a is colloid radius, and exact solutions are given for $f_{\parallel}(h)$ (38) and $f_{\perp}(h)$ (39). Because colloids experience Brownian excursions normal to the surface within potential energy wells, average diffusivities ($\langle D_{\parallel} \rangle, \langle D_{\perp} \rangle$) are given by (34)

$$\langle D \rangle = \int p(h)D(h)dh / \int p(h)dh, \qquad (4)$$

where the desired expression from Eq. 3 is substituted for $D(h)$, and $p(h)$ is obtained either from a measured height histogram or by inverting Eq. 2 using a known potential. Two-dimensional MSDs measured parallel to the underlying surface can be used to evaluate the average lateral diffusivity as $\langle r^2 \rangle = 4\langle D_{\parallel} \rangle t$, where t is time. Lateral migration superimposed on diffusion is well described in MSD data by a parabolic upturn $(Vt)^2$ related to a lateral force, $F = (V/\langle D_{\parallel} \rangle)(kT)$ (40). Partially confined MSD data are fit by an equation of the form, $L^2(1 - C_1 \exp(-C_2\langle D_{\parallel} \rangle t/L^2))$, where L is a confinement length, and C_1 and C_2 are constants that can be related to well shape (40).

Colloid-surface association lifetimes

To a first approximation, the equilibrium CSA lifetime, t_a, depends on diffusion-limited motion of colloids near surfaces and the colloid-surface interaction potential as (41,42)

$$t_a \approx (l^2/\langle D_\perp \rangle)\exp(|u_{min}|/kT), \quad (5)$$

which can be rearranged with $\tau_a = t_a \langle D_\perp \rangle/l^2$ and related directly to the potential well depth as

$$\ln(\tau_a) \approx |u_{min}|/kT, \quad (6)$$

w$(l^2/\langle D_\perp \rangle)$ (from Eqs. 3 and 4) is the characteristic timescale for colloid diffusion normal to the surface within an energy well with a characteristic length scale, l, and $\exp(|u_{min}|/kT)$ is the Boltzmann probability of a colloid remaining in an attractive energy well. Single colloids are considered to be associated with the surface in a given image if their height excursions in the two preceding and following images (five total images) have a standard deviation of $\sigma_h < 1.5$ nm, which is an empirical value obtained for irreversibly deposited colloids on unmodified surfaces.

RESULTS AND DISCUSSION

Levitated colloidal probes

Fig. 1 A displays a typical optical microscopy image of 2.2-μm silica colloids levitated above a glass microscope slide against a gravitational potential by nonspecific interactions of physisorbed BSA and copolymers with exposed PEO moieties. 3D colloidal positions are monitored using VM with half pixel resolution in the x and y directions parallel to the surface (Fig. 1 A) and using TIRM with nanometer resolution in the z direction normal to the surface (Fig. 1 B) (26–28). Nonspecific interactions probed in this work include long-range colloid-surface van der Waals (vdW) attraction (43,44) and macromolecular interactions due to interpenetration and compression (45,46) of adsorbed BSA and PEO copolymer layers (Fig. 1 C). Electrostatic interactions are unimportant due to screening at distances >1 nm in 150 mM physiological ionic strength media.

A limiting case of BSA and PEO mediated colloid-surface interactions occurs when repulsive macromolecular interactions dominate vdW attraction to produce robustly levitated diffusing colloids. Fig. 2 shows results for BSA/APS coated colloids levitated above a PEO5k/OTS coated glass slide. Fig. 2 A shows 25 gray diffusing colloidal random walk trajectories with colored pixels corresponding to the natural logarithm of nondimensional CSA lifetimes, $\ln(\tau_a)$ (see Eq. 6). The inset in Fig. 2 A shows a histogram of all $\ln(\tau_a)$ values with the same color scale as the main plot and frequency normalized by the mode. Fig. 2 B shows ensemble average (red) and single colloid (black) PEP, $u(h)$, with and without the confining gravitational potential. Fig. 2 C shows nondimensional lateral MSDs in the x and y directions versus the nondimensional diffusive time, $\tau_D = t_D \langle D_\| \rangle/a^2$ (see Eq. 4), from an average over all colloids and multiple time origins.

The ensemble average and all single colloid PEP in Fig. 2 B are identical within the limits of polydispersity (26,29,30),
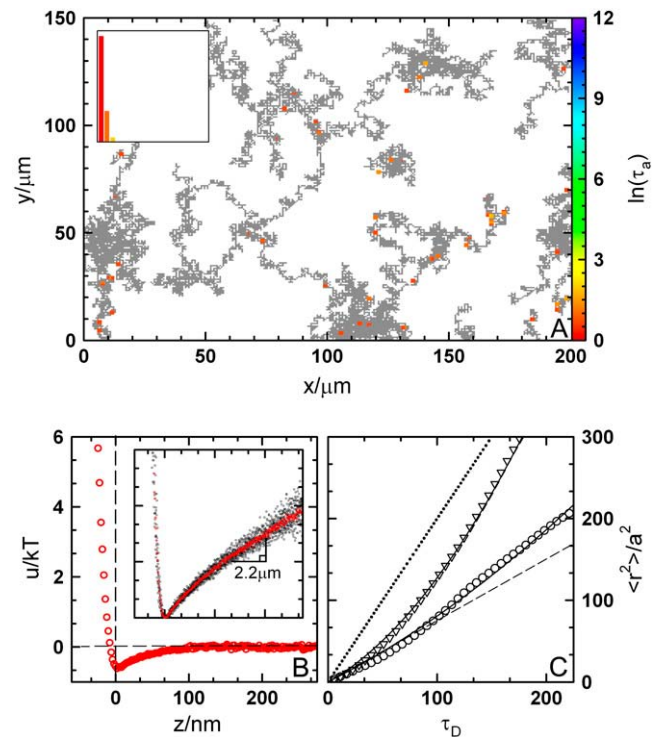

FIGURE 2 (A) Trajectories of BSA/APS-coated colloids on PEO5k/OTS-coated glass surface. Gray pixels indicate no CSA, and colored pixels indicate CSA times (right-side scale). (B) Single (black) and ensemble (red) colloid PEPs with and without gravitational potentials. (C) Ensemble average lateral MSDs in x (○) and y (∇) directions with curve fits (solid line), predictions (dashed line), and isolated single colloid diffusion (dotted line.).

indicating chemically and physically uniform surfaces and a mean colloid radius of $a = 1.11$ μm, in agreement with independent measurements (28). The net PEP can be interpreted as a superposition of colloid-surface vdW attraction and nonspecific BSA-PEO5k osmotic repulsion to produce a $0.7kT$ energy well. Using 20 nm for the PEO5k copolymer brush thickness (46) and assuming prolate ellipsoid BSA molecules are oriented along their 14 nm major axis (47,48), the onset of BSA-PEO repulsion can be expected at 34 nm. By fitting the measured vdW minimum using rigorous theory (43,44), the onset of repulsion is estimated to occur at 40 nm. The vdW attraction, however, is likely to be weakened by surface roughness (44,49) such that occurrence of the 0.7 kT minimum at smaller separations is consistent with a repulsive BSA-PEO interaction at ~34 nm.

Lateral diffusion results in Fig. 2 C provide temporal and spatial information consistent with the predominantly repulsive PEP in Fig. 2 B. As expected, the lateral diffusivity is ~$(1/2)D_0$ due to hydrodynamic interactions between colloids and the underlying wall surface (34). Predicted lateral diffusivities (Eqs. 3 and 4), based on colloid-surface hydrodynamic interactions with impermeable adsorbed layers (50), are in excellent agreement with the short-time x and y MSDs. The parabolic upturn from the initially linear MSD in the

y direction is indicative of migration due to a lateral force $<$ 1 fN, consistent with a misleveling of $< 1°$.

In addition to PEP and diffusivity results in Fig. 2, B and C, the colored pixels in Fig. 2 A indicate $\ln(\tau_a)$ values identified using the analysis described in Materials and Methods. The most probable CSA lifetime is $t_a = 32$ ms from the histogram. This corresponds well to the 0.7 kT well in Fig. 2 B with a diffusion-limited timescale of $l^2/\langle D_\perp \rangle = 16$ ms based on the predicted value of $\langle D_\perp \rangle$ (Eq. 3) and a characteristic diffusive length scale of ~ 14 nm within the energy well (Eq. 6). The value of l is not obvious a priori due to the continuous nature of the attractive interaction, but ~ 14 nm is comparable to the well dimension and gives a reasonable timescale for diffusion-limited motion of levitated colloids in the absence of attraction. The minimal number and duration of association events in Fig. 2 A is consistent with the repulsive PEP in Fig. 2 B that is averaged over all colloids, surface locations, and the total observation period.

A small number of CSA events are observed in Fig. 2 A, but these most likely result from a somewhat conservative criterion for identifying discrete CSA events from probabilistic colloid height excursions. These few CSA events do not obviously correspond to chemical or physical surface heterogeneity that might produce locally stronger attraction. The predominantly gray pixels in Fig. 2 A also indicate temporally and spatially uninterrupted lateral diffusion consistent with the MSDs in Fig. 2 C, which would be significantly retarded in the presence of either more or longer CSA events. All results in Fig. 2 demonstrate characteristics of robust colloidal levitation via net potentials that are mainly repulsive due to long-range, nonspecific interactions of adsorbed BSA and PEO macromolecules.

Irreversibly deposited colloidal probes

At the other extreme of robust colloidal levitation observed in Fig. 2 is the limiting case of irreversible colloidal deposition due to strong colloid-surface attraction. Fig. 3 shows results in this work that most closely approach irreversible deposition for BSA adsorbed to unmodified silica colloids and to 5 nm Au films on a microscope slide. Fig. 3 A shows 22 colloid trajectories in gray with colored pixels indicating $\ln(\tau_a)$ values and an inset histogram of $\ln(\tau_a)$ values similar to Fig. 2 A. Fig. 3 B shows the ensemble average (*red*) and 11 single colloid (*black*) PEP with exponential curve fits to both sides of the ensemble average PEP having decay lengths of $\kappa^{-1} = 5$ nm. Fig. 3 C shows lateral MSD with the same format as in Fig. 2 C.

Results in Fig. 3 show characteristics of irreversibly deposited colloids resulting from colloid-surface vdW attraction dominating short range BSA-BSA repulsion. Adsorbed BSA layers are still expected to have repulsive interactions in Fig. 3, but the range of repulsion is diminished compared to Fig. 2 due to the formation of much thinner, ~ 3 nm, layers on unmodified colloid surfaces (47). Another factor favoring
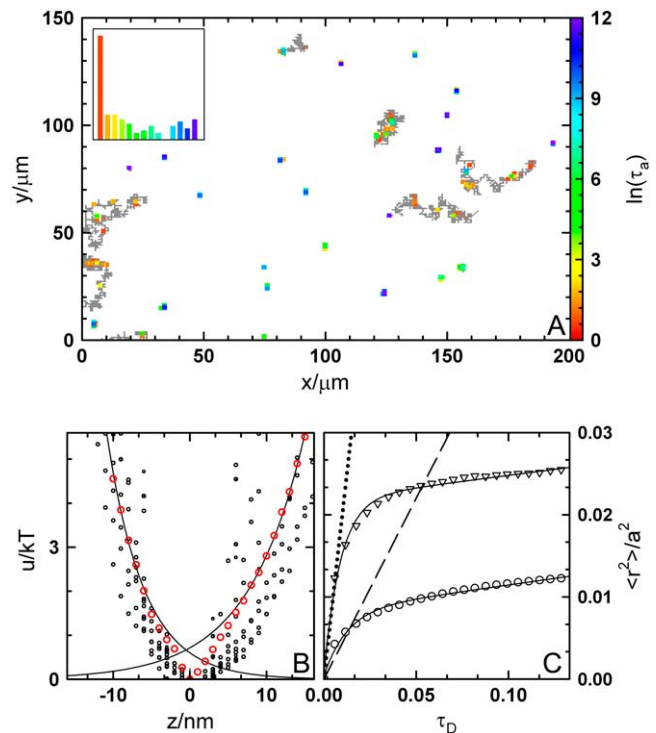

FIGURE 3 (*A*) Trajectories of BSA-coated colloids on BSA/Au-coated glass surface with same format as Fig. 2. (*B*) Single (*black*) and ensemble (*red*) deposited colloid PEPs with exponential curve fits. (*C*) Ensemble average lateral MSDs with same format as Fig. 2.

deposition is an $\sim 5\times$ greater vdW silica-Au attraction in Fig. 3 compared to silica-silica attraction in Fig. 2 (27). As the result of thin adsorbed layers and strong vdW attraction, the ensemble average PEP in Fig. 3 B primarily shows colloids confined to the bottom of energy wells that are deep compared to kT.

Curve fits to lateral MSDs in Fig. 3 C yield confinement lengths of 78 and 127 nm in the x and y directions and short-time $\langle D_\parallel \rangle$ values remarkably similar to predictions (Eq. 4). The latter correspondence is probably somewhat fortuitous given the proximity of the associated length scales to the subpixel limited resolution of our CCD camera. Results in Fig. 3 C also show long-time $\langle D_\parallel \rangle$ is suppressed (except for several weakly associated colloids), which is not obvious a priori because normal particle-surface attraction can still allow lateral diffusion via rolling. Local deformation (51) and interpenetration (52) of adsorbed BSA layers in contact probably provide resistance to translation via rolling. The normal and lateral confinement observed in Fig. 3 C is a general feature of irreversibly deposited colloids, at least in the absence of lateral potential fields.

CSA events reported in Fig. 3 A are a more sensitive measure of colloid deposition than the MSDs in Fig. 3 C due to the significantly better spatial resolution of TIRM compared to VM (~ 1 nm vs. ~ 600 nm). Some explanation is required for the finite colloid-surface dissociation observed

in Fig. 3 *A*, as truly irreversible deposition should produce the trivial result of all colloids being immobilized for the duration of the ~40-min experiment to produce all blue pixels (ln(2.3 × 10⁵ ms/16 ms) ≈ 12 based on Eq. 6 and the diffusion-limited timescale identified in Fig. 2 *A*). The different colored isolated pixels in Fig. 3 *A* result from both apparent height excursions due to signal noise and actual low probability excursions of colloids out of ~12 *kT* wells. For example, any deposited colloid displaying either real or apparent height excursions during the measurement period will overwrite blue pixels (large τ_a) with red-shifted pixels (small τ_a). Overwriting occurs due to lateral confinement, which suggests isolated red-shifted pixels still correspond to nearly irreversibly deposited particles.

Although noise can produce apparent dissociation events, five colloids in Fig. 3 *A* clearly display significant lateral diffusion and short-lived CSA events. Such behavior could arise from locally diminished colloid-surface attraction due to surface nonuniformities (44), smaller colloids within the sample polydispersity (28), and variations in the local BSA layer architecture that generate short range repulsion thereby weakening attraction at contact. In any case, the small percentage of colloid-surface dissociation events and the occurrence of finite lateral diffusivities in Fig. 3 suggest ~12 *kT* deep attractive wells due to residual repulsion between thin BSA layers that, although insufficient for robust stabilization, still significantly weaken vdW attraction compared to bare surfaces in contact. The results in Fig. 3 also suggest attraction can be altered on the *kT* scale in the presence of surface heterogeneity to influence local CSA events.

Associated colloidal probes and surface heterogeneity

Intermediate to the limiting cases of robust levitation and irreversible deposition is the case of intermittent CSA. As captured by Eq. 6, τ_a values are exponentially sensitive to the attractive well depth, u_{min}, and become diffusion limited as $u_{min} \rightarrow 0$ and infinitely long as $u_{min} \rightarrow -\infty$. The nondimensional quantity, u_{min}/kT, indicates the relative magnitudes of attraction favoring CSA and thermal Brownian motion favoring colloid-surface dissociation. As a result, small changes in u_{min} relative to *kT* produce exponentially large changes in τ_a, which is important for understanding intermittent CSA as mediated by adsorbed BSA and PEO layers.

Fig. 4 shows representative results for intermittent CSA with BSA adsorbed to 1-octadecanoic acid ODA-coated silica colloids and PEO3k adsorbed to an OTS-coated glass slide. Each plot in Fig. 4 displays information similar to corresponding plots in Figs. 2 and 3. Fig. 4 *A* shows uninterrupted lateral colloid random walks in some regions and other regions displaying a spectrum of colored pixels indicative of broadly varying τ_a. Fig. 4 *B* shows four single colloid PEPs with solid red lines showing exponential fits
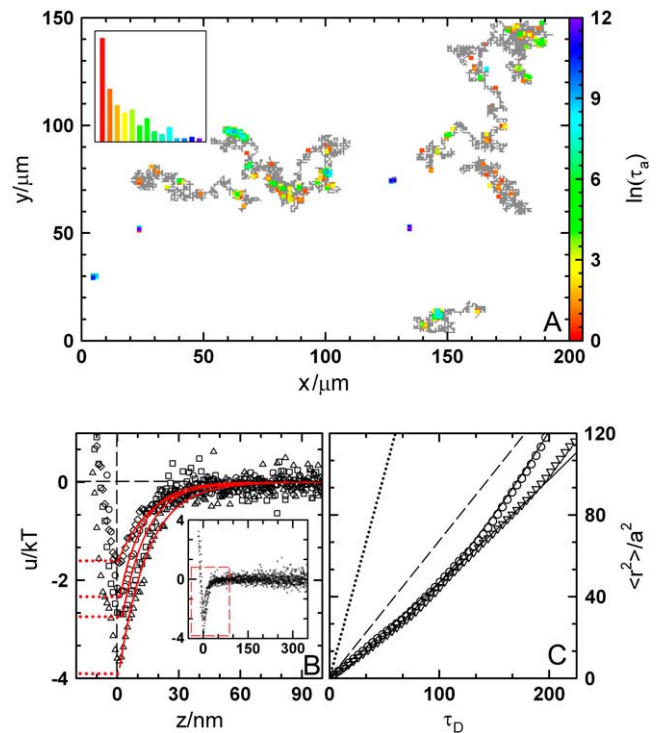

FIGURE 4 (*A*) Trajectories of BSA/ODA-coated colloids on a PEO3k/OTS-coated glass surface with same format as Fig. 2. (*B*) Single colloid PEPs (*black*) without gravitational potentials and exponential curve fits (*red*) to vdW attraction. (*C*) Ensemble average lateral MSDs with same format as Fig. 2.

(12–15 nm decay lengths) to each attractive potential with minima of −1.6, −2.3, −2.7, −3.8 *kT* indicated by dashed red lines.

Results in Fig. 4 *B* indicate varying levels of attraction between BSA-coated colloids and a PEO3k-coated wall that could be misinterpreted without additional information as a novel BSA-PEO attraction. Nevertheless, results in Fig. 4 *A* indicate numerous spatially and temporally distributed CSA events consistent with local attraction on a heterogeneous surface. Because single colloid PEPs in Fig. 4 *B* are constructed by averaging all heights over each colloid's random walk without distinction for its local interaction, the resulting net colloid-surface potentials include both levitated (*gray pixels*) and associated (*colored pixels*) height excursions. As a result, deeper wells are observed in Fig. 4 *B* when a greater proportion of height excursions are measured during associated rather than levitated states. By identifying and discarding the "heterogeneous portion" of each average PEP in Fig. 4 *B*, all single colloid PEPs can be "corrected" to collapse onto a single curve remarkably similar to the PEP in Fig. 2 *B*. This result indicates the BSA-PEO5k and BSA-PEO3k repulsion in Figs. 2 *B* and 4 *B* are similar once effects of surface heterogeneity (that are not concealed by the thinner PEO3k layer) are considered.

The surface heterogeneity implicated in Fig. 4, *A* and *B* is also consistent with the retarded lateral diffusion in Fig. 4 *C*,

which is apparent from the measured diffusivity, $\langle D_\parallel \rangle / D_0 = 0.2$, being less than the predicted diffusivity, $\langle D_\parallel \rangle / D_0 = 0.3$, from Eqs. 3 and 4. Because colloids are already held near the surface in attractive wells, the diminished diffusion cannot be explained by increased hydrodynamic hindrance but is consistent with intermittent CSA events hindering the lateral diffusion process (34). Nearly linear MSD curves in Fig. 4 C also suggest CSA events are spatially random, as anything else would produce characteristic features indicative of diffusion over a periodic landscape (27). The net interpretation of the results in Fig. 4 is that the suspect surface heterogeneity is randomly distributed such that locally varying attraction on the 1 to 10-kT scale produces intermittent CSA events among other regions without any CSA.

The algorithm for identifying discrete association events produces consistent results for experiments in Figs. 2–4 involving levitation, association, and deposition of BSA- and PEO-coated colloids on similarly coated surfaces. Because the statistical nature of CSA events does not allow an a priori method for identifying discrete CSA events, a certain fraction of measurements are designated in error as either levitated or associated in all cases. Yet, the validity of the algorithm is justified a posteriori because using more or less conservative constraints begin to distort PEPs from agreement with independent measures (e.g., colloid radius via the gravitational potential, colloid diffusivity via Eq. 4). By neither removing too many points corresponding to homogeneous vdW interactions (to underestimate the attractive well) nor leaving too many points corresponding to heterogeneous association events (to overestimate the attractive well) the algorithm for identifying CSA events produces self-consistent, energetic, spatial, statistical, and temporal results in Figs. 2–4.

Colloidal probe nonuniformity and migration

Although wall surface heterogeneity appears to be implicated in the intermittent CSA results in Figs. 3 and 4, there is no obvious indication of colloid nonuniformity. Colloids likely have molecular-scale heterogeneity (53) but also appear to be sufficiently uniform that they can be analyzed as ensembles (26), which was an unstated assumption up to this point. For comparison, Fig. 5 reports a unique experiment involving a single outlier colloid with similar plots to Figs. 2–4. Results are shown for BSA/APS-coated colloids levitated above a BSA/APS-coated glass slide. The flow cell was intentionally misleveled in Fig. 5 upon observation of the outlier colloid to observe surface association in the presence of lateral migration.

The obvious departure of the single predominantly orange-yellow-green trajectory in Fig. 5 A from all other gray trajectories allows for its straightforward identification and its separate analysis from the otherwise robustly levitated colloids. Because the trajectory of the outlier colloid coincides with the same surface locations as a preceding
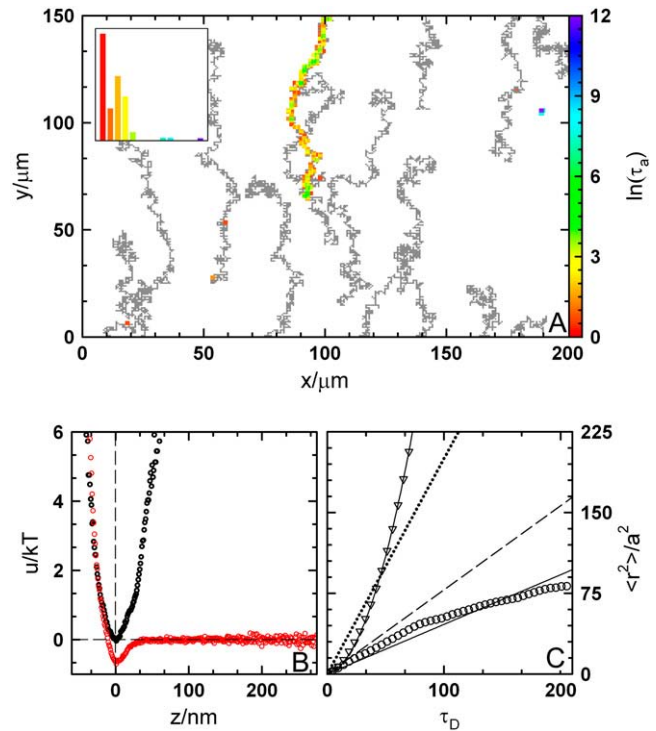

FIGURE 5 (A) Trajectories of BSA/APScoated colloids on a BSA/APS-coated glass surface with same format as Fig. 2. (B) Single associating colloid (*black*) and ensemble (*red*) colloid PEPs without gravitational potentials. (C) Ensemble average lateral MSDs with same format as Fig. 2.

colloid's trajectory, the frequent intermittent association of the outlier colloid with the surface can be attributed to defects on the colloid rather than the wall. The red PEP in Fig. 5 B is the ensemble average profile of 13 colloids excluding the outlier colloid and is typical for robustly levitated colloids (see Fig. 2 B). The black PEP in Fig. 5 B corresponds to the single outlier colloid and displays the parabolic shape characteristic of deposited colloids (Fig. 3) except for its greater width due to larger height excursions. Results in Fig. 5 B demonstrate BSA-BSA mediated colloid-surface interaction can be quantified in the presence of migration and an easily identifiable deviant colloid to produce ~ 0.7 kT attractive vdW well similar to the BSA-PEO5k PEP in Fig. 2 B.

Fig. 5 C shows a parabolic upturn in the MSD in the y direction consistent with the obvious migration in Fig. 5 A, whereas the MSD in the x direction shows a turnover approaching a constant MSD that is indicative of confinement. Because the colloids should not be confined for any obvious reasons, the turnover in the x MSD is attributed to migration into or out of the window in the y direction leaving suitably sampled short-time trajectory data but statistically deficient long-time data. Analysis of the migration in Fig. 5 C indicates an $\sim 5°$ tilt in the flow cell based on a component of gravity acting parallel to the surface. The lateral migration of the associating outlier colloid in Fig. 5 does not appear to be hindered by any tangential interaction in contrast to the

diffusive behavior in Fig. 3, which might result from the lateral force exceeding a sort of tangential yield stress. As a side note, the colloid migration in Fig. 5 is reminiscent of ligand coated colloids and leukocytes on surfaces (54), which suggests another potentially interesting application for investigation with the new methods reported here.

The outlier colloid's greater association with the surface could result from defects due to the APS silanization procedure, which is performed under metastable conditions such that periodic aggregate formation could produce surface patches altering the local interaction. Observation of non-uniform colloids was also extremely rare; for ~20 colloids interrogated in nearly 100 ensemble experiments similar to Figs. 2–5, only the single outlier colloid in Fig. 5 was observed, suggesting an occurrence of $< \sim 1/2000$. Based on the results in this work, nonuniform colloids are rarely observed in comparison to wall surface heterogeneity.

BSA-PEO interactions and surface heterogeneity

The results in Figs. 2–5 demonstrate the ability to simultaneously observe many single colloids interacting with different surface regions. By averaging over many colloids and surface positions, statistically significant results are obtained but not at the expense of losing discrete information about single colloids and local surface properties. Table 1 summarizes several trends that emerge from numerous systematic measurements of BSA- and PEO-coated colloids and surfaces and reports average $\ln(\tau_a)$ values for 25 experiments performed in triplicate including: 1), BSA adsorbed to APS modified colloids and surfaces, 2), BSA, PEO5k, PEO4k, and PEO3k adsorbed to ODA modified silica colloids and OTS modified microscope slides. The $\ln(\tau_a)$ values in Table 1 are averaged over all colloids, surface locations, and observation time (i.e., average over all gray and colored pixels in Figs. 2–5).

Effects of adsorbed macromolecule molecular weight on $\ln(\tau_a)$ values are apparent from the PEO-PEO layer interactions in Table 1. For example, the highest molecular weight PEO5k copolymer absorbed to OTS- and ODA-modified surfaces yield ~20-nm thick layers (46) that are expected to produce the observed robust levitation ($\ln(\tau_a) = 0.8$). In contrast, adsorption of ~10 nm PEO3k layers (55) to similarly modified surfaces allows significantly more and longer lived

CSA events ($\ln(\tau_a) = 3.5$). The general trend that emerges in Table 1 is that thicker layers due to higher PEO molecular weights produce smaller $\ln(\tau_a)$ values. Because all PEO copolymers have similar triblock ratios, their adsorbed layers are expected to have brush architectures with thicknesses determined primarily by molecular weight (52). PEO interactions are also expected to be purely repulsive for the favorable solvent conditions explored in this work (46). A likely mechanism leading to decreasing $\ln(\tau_a)$ with increasing PEO molecular weight is that thicker layers are more likely to conceal chemical and physical surface heterogeneities that allow for increased local attraction and CSA.

Effects of adsorbed layer architecture in Table 1 can be deduced from the BSA-BSA data, which consist of monodisperse macromolecules adsorbed with different orientations on different chemically modified surfaces. For example, adsorption of BSA to APS modified silica can produce ~14 nm thick layers via a preferred orientation of BSA parallel to its major axis (48) to produce robust levitation ($\ln(\tau_a) = 0.6$). In contrast, adsorption of BSA to OTS-modified silica surfaces can produce thin ~3 nm layers via a flatter BSA orientation (14) to yield significantly more and longer lived CSA events ($\ln(\tau_a) = 6.8$). BSA conformation may also be perturbed on different chemically modified surfaces to influence adsorbed layer thicknesses. The BSA-BSA data in Table 1 suggest that thicker layers via architectural effects can also better conceal surface heterogeneities similar to PEO molecular weight effects.

Finally, for the asymmetric BSA-PEO interactions in Table 1, the $\ln(\tau_a)$ data can be explained based on the concealment of surface heterogeneity due to a combination of PEO molecular weight and BSA orientation. For example, BSA/APS-modified surfaces interacting with PEO5k/OTS-ODA surfaces produce robust levitation ($\ln(\tau_a) = 3.2, 2.4$) whereas BSA and PEO3k adsorbed to alkyl-modified surfaces produce comparatively more and longer CSA events ($\ln(\tau_a) = 9.3, 5.3$). In all cases, BSA-PEO interactions are completely repulsive, consistent with standard theories for macromolecular interactions in good solvent conditions. As a result, adsorbed BSA and PEO layers can robustly levitate colloids above surfaces provided layers are thick enough to overcome colloid-surface attraction, particularly in the presence of surface heterogeneity.

A final note about the data in Table 1 is that they are not symmetric about the diagonal; there is a bias toward greater $\ln(\tau_a)$ for thin adsorbed layers on the colloid instead of the wall. For example, PEO3k adsorbed to colloids interacting with BSA/APS-coated walls experience longer CSA lifetimes with $\ln(\tau_a) = 9.3$ than the reverse case with $\ln(\tau_a) = 5.3$. The simplest explanation for this bias is differences in the colloid and wall surface modifications. Because stable silica colloids are modified with ODA using a well-established method (36), the problem is expected to lie with OTS modification of the glass slide surface, which is known to produce OTS aggregates (35) (surface roughness under < 5 nm

TABLE 1 Summary of $\ln(\tau_a)$ values for combinations of colloids and surfaces with adsorbed BSA and PEO copolymers

Colloid \ Wall	BSA/APS	PEO5k	PEO4k	PEO3k	BSA/OTS
BSA/APS	0.6	2.4	4.4	5.3	5.1
PEO5k	3.2	0.8	2.3	1.4	2.6
PEO4k	5.4	1.3	2.0	4.2	2.5
PEO3k	9.3	2.6	2.5	3.5	3.2
BSA/OTA	10.2	4.4	5.0	5.4	6.8

does not significantly scatter the evanescent wave) (44). The dielectric properties of aggregated alkane structures on the wall could reduce vdW attraction compared to alkane layers on colloids (43), which would produce the observed bias toward greater $\ln(\tau_a)$ for thin adsorbed layers on the colloid compared to the wall.

SUMMARY AND CONCLUSIONS

This article describes a distinctly new approach for quantitatively measuring interactions of proteins and synthetic macromolecules adsorbed to colloids and wall surfaces. Using an integrated TIRM and VM colloid tracking technique, equilibrium and dynamic analyses of the 3D trajectories of many freely diffusing colloids provide simultaneous energetic, spatial, statistical, and temporal information about adsorbed BSA and PEO copolymer interactions. Information from such measurements includes single colloid and ensemble average PEP, lateral diffusivities, and CSA lifetimes. A consistent analysis of such information in several demonstrative measurements is used to distinguish different colloid-surface interaction regimes as belonging to levitation, association, or deposition.

This newly developed method and associated analyses were then employed in a systematic series of experiments to capture how average colloid-surface interactions are mediated by combinations of chemical surface modifications, adsorbed BSA and PEO layers, and surface heterogeneity. These results reveal how BSA layer architecture on different chemically modified substrates and PEO copolymer molecular weight together either conceal or expose underlying substrate heterogeneities to influence colloid-surface attraction and association lifetimes. In all cases, BSA-BSA, BSA-PEO, and PEO-PEO interactions appear to be completely repulsive such that CSA only occurs due to nonspecific colloid-surface attraction, particularly in the presence of surface heterogeneity. The results in this work demonstrate nonspecific repulsion of proteins and synthetic macromolecules as a basis for creating integrated biomolecular-synthetic devices and as a baseline to differentiate specific and nonspecific interactions between protein binding partners on colloids and surfaces.

REFERENCES

1. Langer, R., and N. A. Peppas. 2003. Advances in biomaterials, drug delivery, and bionanotechnology. *AIChE J.* 49:2990–3006.

2. West, J. L., and N. J. Halas. 2003. Engineered nanomaterials for biophotonics applications: improving sensing, imaging, and therapeutics. *Ann. Rev. Biomed. Eng.* 5:285–292.

3. Leckband, D., and J. Israelachvili. 2001. Intermolecular forces in biology. *Q. Rev. Biophys.* 34:105–267.

4. Leckband, D. 2000. Measuring the forces that control protein interactions. *Annu. Rev. Biophys. Biomol. Struct.* 29:1–26.

5. Evans, E. 2001. Probing the relation between force-lifetime-and chemistry in single molecular bonds. *Annu. Rev. Biophys. Struct.* 30: 105–128.

6. Bustamante, C., Y. R. Chemla, N. R. Forde, and D. Izhaky. 2004. Mechanical processes in biochemistry. *Annu. Rev. Biochem.* 73:705–748.

7. Rohrbach, A., C. Tischer, D. Neumayer, Ernst-Ludwig Florin, and E. H. K. Stelzer. 2004. Trapping and tracking a local probe with a photonic force microscope. *Rev. Sci. Inst.* 75:2197–2210.

8. Horber, J. K. H., and M. J. Miles. 2003. Scanning probe evolution in biology. *Science.* 302:1002–1005.

9. Patra, M., and P. Linse. 2006. Simulation of grafted polymers on nanopatterned surfaces. *Nano Lett.* 6:133–137.

10. Patra, M., and P. Linse. 2006. Reorganization of nanopatterned polymer brushes by the AFM measurement process. *Macromolecules.* 39:4540–4546.

11. Sheth, S. R., and D. Leckband. 1997. Measurement of attractive forces between proteins and end-grafted poly(ethylene glycol) chains. *Proc. Natl. Acad. Sci. USA.* 94:8399–8404.

12. Vijayendran, R. A., and D. E. Leckband. 2001. A quantitative assessment of heterogeneity for surface-immobilized proteins. *Anal. Chem.* 73:471–480.

13. Schuster, S. C., R. V. Swanson, L. A. Alex, R. B. Bourret, and M. I. Simon. 1993. Assmebly and function of a quaternary signal transduction complex monitored by surface plasmon resonance. *Nature.* 365: 343–347.

14. Wertz, C. F., and M. M. Santore. 2001. Effect of surface hydrophobicity on adsorption and relaxation kinetics of albumin and fibrinogen: single-species and competitive behavior. *Langmuir.* 17:3006–3016.

15. Schuck, P. 1997. Use of surface plasmon resonance to probe the equilibrium and dynamic aspects of interactions between biological macromolecules. *Annu. Rev. Biophys. Biomol. Struct.* 26:541–566.

16. Smith, E. A., and R. M. Corn. 2003. Surface plasmon resonance imaging as a tool to monitor biomolecular interactions in an array based format. *Appl. Spectrosc.* 57:320A–332A.

17. Shumaker-Parry, J. S., and C. T. Campbell. 2004. Quantitative methods for spatially resolved adsorption/desorption measurements in real time by surface plasmon resonance microscopy. *Anal. Chem.* 76: 907–917.

18. Brockman, J. M., B. P. Nelson, and R. M. Corn. 2000. Surface plasmon resonance imaging measurements of ultrthin organic films. *Annu. Rev. Phys. Chem.* 51:41–63.

19. Liebert, R. B., and D. C. Prieve. 1995. Species-specific long range interactions between receptor/ligand pairs. *Biophys. J.* 69:66–73.

20. Robertson, S. K., and S. G. Bike. 1998. Quantifying cell-surface interactions using model cells and total internal reflection microscopy. *Langmuir.* 14:928–934.

21. Robertson, S. K., A. F. Uhrick, and S. G. Bike. 1998. TIRM measurements with cells and liposomes. *J. Colloid Interface Sci.* 202: 208–211.

22. Singh-Zocchi, M., S. Dixit, V. Ivanov, and G. Zocchi. 2003. Single-molecule detection of DNA hybridization. *Proc. Natl. Acad. Sci. USA.* 100:7605–7610.

23. Schilling, J., K. Sengupta, S. Goennenwein, A. R. Bausch, and E. Sackmann. 2004. Absolute interfacial distance measurements by dual-wavelength reflection interference contrast microscopy. *Phys. Rev. E.* 69:021901.

24. Gelles, J., B. J. Schnapp, and M. P. Sheetz. 1988. Tracking kinesin-driven movements with nanometer-scale precision. *Nature.* 331:450–453.

25. Schafer, D. A., J. Gelles, M. P. Sheetz, and R. Landick. 1991. Transcription by single molecules of RNA polymerase observed by light microscopy. *Nature.* 352:444–448.

26. Wu, H. J., and M. A. Bevan. 2005. Direct measurement of single and ensemble average particle-surface potential energy profiles. *Langmuir.* 21:1244–1254.

27. Wu, H.-J., W. N. Everett, S. G. Anekal, and M. A. Bevan. 2006. Mapping patterned potential energy landscapes with diffusing colloidal probes. *Langmuir.* 22:6826–6836.

28. Wu, H.-J., T. O. Pangburn, R. E. Beckham, and M. A. Bevan. 2005. Particle-particle & particle-wall interactions in levitated colloidal ensembles. *Langmuir.* 21:9879–9888.

29. Pangburn, T. O., and M. A. Bevan. 2005. Role of polydispersity in anomalous interactions in electrostatically levitated colloidal systems. *J. Chem. Phys.* 123:174904.

30. Pangburn, T. O., and M. A. Bevan. 2006. Anomalous potentials from inverse analyses of interfacial polydisperse attractive colloidal fluids. *J. Chem. Phys.* 124:054712.

31. Lu, M., M. A. Bevan, and D. M. Ford. 2005. Inverse density-functional theory as an interpretive tool for measuring colloid-surface interactions in dense systems. *J. Chem. Phys.* 122:224710.

32. Bevan, M. A., and D. C. Prieve. 2000. Hindered diffusion of colloidal particles very near to a wall. *Revisited. J. Chem. Phys.* 113:1228–1236.

33. Anekal, S., and M. A. Bevan. 2005. Interpretation of conservative forces from stokesian dynamic simulations of interfacial and confined colloids. *J. Chem. Phys.* 122:034903.

34. Anekal, S., and M. A. Bevan. 2006. Self diffusion in sub-monlayer colloidal fluids near a wall. *J. Chem. Phys.* 125:034906.

35. Ulman, A. 1996. Formation and structure of self assembled monolayers. *Chem. Rev.* 96:1553–1554.

36. van Helden, A. K., J. W. Jansen, and A. Vrij. 1981. Preparation and Characterization of Spherical Monodisperse Silica Dispersions in Non-Aqueous Solvents. *J. Colloid Interface Sci.* 81:354–368.

37. Prieve, D. C. 1999. Measurement of colloidal forces with TIRM. *Adv. Colloid Interface Sci.* 82:93–125.

38. Goldman, A. J., R. G. Cox, and H. Brenner. 1967. Slow viscous motion of a sphere parallel to a plane wall–i. motion through a quiescent fluid. *Chem. Engr. Sci.* 22:637–651.

39. Brenner, H. 1961. The slow motion of a sphere through a viscous fluid towards a plane surface. *Chem. Eng. Sci.* 16:242–251.

40. Saxton, M. J., and K. Jacobson. 1997. Single-particle tracking: applications to membrane dynamics. *Annu. Rev. Biophys. Biomol. Struct.* 26:373–399.

41. Chandrasekhar, S. 1943. Stochastic problems in physics and astronomy. *Rev. Mod. Phys.* 15:1–89.

42. Hanggi, P., and P. Talkner. 1990. Reaction-rate theory: fifty years after Kramers. *Rev. Mod. Phys.* 62:251–341.

43. Parsegian, V. A. 2005. Van der Waals Forces. Cambridge University Press, Cambridge.

44. Bevan, M. A., and D. C. Prieve. 1999. Direct measurement of retarded van der Waals attraction. *Langmuir.* 15:7925–7936.

45. Israelachvili, J. N. 1992. Intermolecular and Surface Forces. Academic Press, New York.

46. Bevan, M. A., and D. C. Prieve. 2000. Forces and hydrodynamic interactions between polystyrene surfaces with adsorbed PEO-PPO-PEO. *Langmuir.* 16:9274–9281.

47. Bendedouch, D., and S. H. Chen. 1983. Structure and interparticle interactions of bovine serum albumin in solution studied by small-angle neutron scattering. *J. Phys. Chem.* 87:1473–1477.

48. Kurrat, R., J. E. Prenosil, and J. J. Ramsden. 1997. Kinetics of human and bovine serum albumin adsorption at silica-titania surfaces. *J. Colloid Interface Sci.* 185:1–8.

49. Dagastine, R. R., M. A. Bevan, L. R. White, and D. C. Prieve. 2004. Calculation of van der Waals forces with diffuse coatings: applications to roughness and adsorbed polymers. *J. Adhesion.* 80:365–394.

50. Potanin, A. A., and W. B. Russel. 1995. Hydordynamic interaction of particles with grafted polymer brushes and applications to rheology of colloidal dispersions. *Phys. Rev. E.* 52:730–737.

51. Johnson, K. L., K. Kendall, and A. D. Roberts. 1971. Surface energy and the contact of elastic solids. *Proc. R. Soc. Lond. A.* 324:301–313.

52. Fleer, G. J., M. A. C. Stuart, J. M. H. M. Scheutjens, T. Cosgrove, and B. Vincent. 1993. Polymers at interfaces. Chapman & Hall, New York.

53. Feick, J. D., and D. Velegol. 2002. Measurements of charge nonuniformity on polystyrene latex particles. *Langmuir.* 18:3454–3458.

54. Hammer, D. A., and S. M. Apte. 1992. Simulation of cell rolling and adhesion on surfaces in shear-flow general results and analysis of selectin-mediated neutrophil adhesion. *Biophys. J.* 63:35–57.

55. Baker, J. A., and J. C. Berg. 1988. Investigation of the adsorption configuration of poly(ethylene oxide) and its copolymers with poly(propylene oxide) on model polystyrene latex dispersions. *Langmuir.* 4:1055–1061.